HAL open science

Antiviral activity of oleandrin and a defined extract of Nerium oleander against SARS-CoV-2

Kenneth Plante, Varun Dwivedi, Jessica Plante, Diana Fernandez, Divya Mirchandani, Nathen Bopp, Patricia Aguilar, Jun-Gyu Park, Paula Pino Tamayo, Jennifer Delgado, et al.

To cite this version:

Kenneth Plante, Varun Dwivedi, Jessica Plante, Diana Fernandez, Divya Mirchandani, et al.. Antiviral activity of oleandrin and a defined extract of Nerium oleander against SARS-CoV-2. Biomedicine and Pharmacotherapy, 2021, 138, pp.111457. ⟨10.1016/j.biopha.2021.111457⟩. ⟨hal-03213218⟩

HAL Id: hal-03213218

https://hal.inrae.fr/hal-03213218v1

Submitted on 30 Apr 2021

HAL is a multi-disciplinary open access archive for the deposit and dissemination of scientific research documents, whether they are published or not. The documents may come from teaching and research institutions in France or abroad, or from public or private research centers.

L'archive ouverte pluridisciplinaire **HAL**, est destinée au dépôt et à la diffusion de documents scientifiques de niveau recherche, publiés ou non, émanant des établissements d'enseignement et de recherche français ou étrangers, des laboratoires publics ou privés.

Distributed under a Creative Commons CC BY 4.0 - Attribution - International License

Biomedicine & Pharmacotherapy 138 (2021) 111457

Contents lists available at ScienceDirect

Biomedicine & Pharmacotherapy

journal homepage: www.elsevier.com/locate/biopha

Original article

Antiviral activity of oleandrin and a defined extract of *Nerium oleander* against SARS-CoV-2

Kenneth S. Plante [a,b,c,1], Varun Dwivedi [d,1], Jessica A. Plante [a,b,c], Diana Fernandez [a,b,e], Divya Mirchandani [a,b,c], Nathen Bopp [a,b,c], Patricia V. Aguilar [a,b,c,f], Jun-Gyu Park [d], Paula Pino Tamayo [d], Jennifer Delgado [d], Vinay Shivanna [d], Jordi B. Torrelles [d], Luis Martinez-Sobrido [d], Rick Matos [h,j], Scott C. Weaver [a,b,c,f,1], K. Jagannadha Sastry [g,1], Robert A. Newman [i,j,*,1]

[a] World Reference Center for Emerging Viruses and Arboviruses, University of Texas Medical Branch, Galveston, TX 77555, USA
[b] Institute for Human Infections and Immunity, University of Texas Medical Branch, Galveston, TX 77555, USA
[c] Department of Microbiology and Immunology, University of Texas Medical Branch, Galveston, TX 77555, USA
[d] Population Health and Host-Pathogens Interactions Programs, Texas Biomedical Research Institute, San Antonio, TX 78227, USA
[e] Center for Tropical Diseases, University of Texas Medical Branch, Galveston, TX 77555, USA
[f] Department of Pathology, University of Texas Medical Branch, Galveston, TX 77555, USA
[g] Department of Thoracic/Head and Neck Medical Oncology, University of Texas MD Anderson Cancer Center, Houston, TX 77030, USA
[h] Innovar, LLC, Plano, TX 75025, USA
[i] Department of Experimental Therapeutics, University of Texas MD Anderson Cancer Center, Houston, TX 77030, USA
[j] Phoenix Biotechnology, Inc., San Antonio, TX 78217, USA

ARTICLE INFO

Keywords:
Oleandrin
Nerium oleander
SARS-CoV-2
COVID-19
Antiviral activity
Reduced infectivity

ABSTRACT

With continued expansion of the coronavirus disease (COVID-19) pandemic, caused by severe acute respiratory syndrome 2 (SARS-CoV-2), both antiviral drugs as well as effective vaccines are desperately needed to treat patients at high risk of life-threatening disease. Here, we present *in vitro* evidence for significant inhibition of SARS-CoV-2 by oleandrin and a defined extract of *N. oleander* (designated as PBI-06150). Using Vero cells, we found that prophylactic (pre-infection) oleandrin (as either the pure compound or as the active principal ingredient in PBI-06150) administration at concentrations as low as 0.05 μg/ml exhibited potent antiviral activity against SARS-CoV-2, with an 800-fold reduction in virus production, and a 0.1 μg/ml concentration resulted in a greater than 3000-fold reduction in infectious virus production. The half maximal effective concentration (EC_{50}) values were 11.98 ng/ml when virus output was measured at 24 h post-infection, and 7.07 ng/ml measured at 48 h post-infection. Therapeutic (post-infection) treatment up to 24 h after SARS-CoV-2 infection of Vero cells also reduced viral titers, with 0.1 μg/ml and 0.05 μg/ml concentrations causing greater than 100-fold reduction as measured at 48 h, and the 0.05 μg/ml concentration resulting in a 78-fold reduction. Concentrations of oleandrin up to 10 μg/ml were well tolerated in Vero cells. We also present *in vivo* evidence of the safety and efficacy of defined *N. oleander* extract (PBI-06150), which was administered to golden Syrian hamsters in a preparation containing as high as 130 μg/ml of oleandrin. In comparison to administration of control vehicle, PBI-06150 provided a statistically significant reduction of the viral titer in the nasal turbinates (nasal conchae). The potent prophylactic and therapeutic antiviral activities demonstrated here, together with initial evidence of its safety and efficacy in a relevant hamster model of COVID-19, support the further development of oleandrin

Abbreviations: SARS, severe acute respiratory syndrome; MERS, middle east respiratory syndrome; HIV, human immunodeficiency virus; HTLV-1, human T-lymphotropic virus; Mab, monoclonal antibody; NP, nucleocapsid protein; BSA, bovine serum albumin; DPI, day post infection; DMSO, dimethyl sulfoxide; CPE, cytopathic effect; PFU, plaque-forming unit; EC_{50}, half maximal effective concentration; ATP, adenosine triphosphate; Nrf-2, nuclear factor erythroid 2-related factor 2; BDNF, brain-derived neurotrophic factor; FBS, fetal bovine serum; LDH, lactic dehydrogenase; DPBS, Dulbecco's phosphate-buffered saline; qRT-PCR, real-time quantitative polymerase chain reaction; RNA, ribonucleic acid; ALT, alanine transaminase; ALP, alkaline phosphatase; ELISA, enzyme-linked immunoassay; H&E, hematoxylin and eosin.

* Correspondence to: Phoenix Biotechnology, Inc., 8626 Tesoro Dr., Suite 801, San Antonio, TX 78217, USA.
E-mail address: rnewman@phoenixbiotechnology.com (R.A. Newman).

[1] These authors contributed equally to this paper.

https://doi.org/10.1016/j.biopha.2021.111457
Received 24 January 2021; Received in revised form 25 February 2021; Accepted 27 February 2021
Available online 3 March 2021
0753-3322/© 2021 Phoenix Biotechnology, Inc. Published by Elsevier Masson SAS. This is an open access article under the CC BY license (http://creativecommons.org/licenses/by/4.0/).

and/or defined extracts containing this molecule for the treatment of SARS-CoV-2 and associated COVID-19 disease and potentially also for reduction of virus spread by persons diagnosed early after infection.

1. Introduction

After its emergence in late 2019, an epidemic of coronavirus disease termed coronavirus disease 2019 (COVID-19) caused by severe acute respiratory syndrome coronavirus 2 (SARS-CoV-2) was first recognized in the city of Wuhan, China, then quickly spread to pandemic proportions [1]. As of January 2021, over 93 million cases have been identified with nearly every country involved worldwide. The virus has resulted in over 2.0 million human fatalities [2]. Hospitals and other health care systems were overwhelmed in Wuhan, Italy, Spain and New York City before cases peaked in these locations. The underlying virulence of this newly emerged COVID-19 is particularly severe for older age groups and those with chronic pulmonary and cardiac conditions, diabetes, and other comorbidities. Other factors fueling morbidity and mortality have included limited supplies in personal protective devices and ventilators required for endotracheal intubation [3]. While several approved vaccines are now available, their dissemination around the world and administration remain a significant challenge. Moreover, it is possible that vaccines may require continuous redevelopment due to the ongoing mutation of coronavirus into different variants; in addition, the rate of reduction in the titer of neutralizing antibodies remains unclear. Ideally, a SARS-CoV-2 vaccine would induce long-lasting antibodies, but it is not yet known how long specific antibodies persist in SARS-CoV-2 infected individuals or how long they would persist after vaccination [4]. Furthermore, except for Remdesivir, many of the existing antiviral drugs tested to date have shown limited or no efficacy in clinical trials [5–9]. Thus, identification of safe and effective therapeutic agents that can be effective against SARS-CoV-2 remains an unmet need.

Typically, the fastest route to identifying and commercializing a safe and effective antiviral drug is to test those already shown to be safe in early clinical trials for other infections or diseases. A few Food and Drug Administration approved drugs such as Lopinavir-ritonavir, hydroxychloroquine sulfate, and emtricitabine-tenofovir that target human proteins predicted to interact with SARS-CoV-2 proteins showed antiviral activity *in vitro*, yet only marginally reduced clinical outcomes of infected ferrets and did not significantly reduce viral loads [10]. Additionally, several drugs including ribavirin, interferon, lopinavir-ritonavir, and corticosteroids have been used in patients infected with the closely related Beta coronaviruses SARS-CoV, responsible for the 2002–2004 outbreak of respiratory disease, or middle east respiratory syndrome (MERS), responsible for the 2012 outbreak, with varying efficacy results [11].

The class of compounds known as cardenolides consists of well characterized molecules such as digoxin, digitoxin, lanatoside C, ouabain and oleandrin. The mechanism of action for these compounds lies in their ability to inhibit functioning of Na, K-ATPase which alters ion flux across membranes [12], which, in turn, creates an ion imbalance across cellular and perinuclear membranes. This explains the ability of this class of compounds to improve functioning of heart muscle in patients with congestive heart failure by increasing intracellular calcium concentration. In the last several decades, additional therapeutic uses of compounds such as oleandrin have been recognized. These include the use of oleandrin and extracts of the oleander (*N. oleander*) plant containing oleandrin, as effective therapeutics that range from cosmetic treatment of skincare problems [13] to the treatment of cancer [14–16]. Oleandrin, a unique lipid-soluble cardiac glycoside obtained solely from *Nerium oleander*, has been recognized as the active principal ingredient in PBI-05204 used in Phase I and Phase II clinical trials of patients with cancer [17,18]. These trials defined the pharmacokinetics of oleandrin and demonstrated that extracts containing this molecule, along with other components found in the extract, can be administered safely as an oral drug to patients without significant adverse events.

Less appreciated is the antiviral activity of this class of compounds. Recent reviews have described antiviral activities of cardenolides, such as oleandrin, against cytomegalovirus, Herpes simplex virus, adenovirus, chikungunya virus, coronaviruses, respiratory syncytial virus, Ebola virus, influenza virus and human immunodeficiency virus [19, 20]. We recently reported that oleandrin also has strong antiviral activity against HIV-1 and HTLV-1 [21,22]. In studies with HIV-1, a unique antiviral activity of oleandrin was observed in terms of producing viral progeny with a greatly diminished potential to infect new target cells [21]. This decreased infectivity was due in part to a reduction in the gp120 envelope glycoprotein of progeny virus, which is essential for viral infectivity. We also reported that oleandrin treatment of cells infected with HTLV-1 resulted in reduced infectivity of progeny virus particles. Oleandrin inhibited virological synapse formation and consequent transmission of HTLV-1 *in vitro* [22]. Collectively these studies suggest that oleandrin and defined plant extracts containing this molecule have potential against "enveloped" viruses. Because SARS-CoV-2 is also an "enveloped" virus, it was reasoned that oleandrin could be effective in reducing viral load in infected individuals *via* production of progeny virus with a significantly reduced potential to infect new target/host cells, and therefore help with control of the COVID-19 pandemic.

Considering the urgent need to identify potential antiviral therapies for COVID-19, we tested oleandrin in SARS-CoV-2-infected African Green monkey kidney Vero cells at concentrations ranging from 100 μg/ml to 0.005 μg/ml. Here, we demonstrate the strong inhibitory profile of oleandrin in greatly reducing infectious virus production. In addition, the relative safety/toxicity of PBI-06150 was determined in golden Syrian hamsters which have recently been used as a relevant animal model for SARS-CoV-2 infection and pathology to examine antiviral efficacy of proposed therapeutic agents against SARS-CoV-2 infection [23]. In that same study, a statistically significant improvement in reduction of viral load in the nasal turbinates of the hamsters was observed when comparing treated and untreated animals.

2. Materials and methods

2.1. Cells, viruses, and oleandrin

SARS-CoV-2, USA-WA1/2020 strain (Gen Bank: MN985325.1) was obtained from BEI Resources (NR-52281). Passage 6 (P6) of SARS-CoV-2 was generated by infecting Vero E6 cells obtained from the American Type Culture Collection (ATCC, CRL-1586) for 72 h. At 72 h post-infection, tissue culture supernatants were collected, clarified, aliquoted, and stored at − 80 °C. A standard plaque assay (plaque forming units, PFU/ml) in Vero E6 cells was used to titrate P6 (7.9×10^6 PFU/ml) viral stocks. P6 working stock was completely sequenced, using next generation sequencing (NGS), and was 100% identical to the original stock without deletions or mutations compromising virus infectivity as provided by BEI Resources. We examined both our viral master seed and working stocks for single nucleotide variants (SNVs) with a particular emphasis on those impacting the furin-like cleavage site, which has been described to influence the ability of SARS-CoV-2 to transmit between species [24,25]. Our results confirmed that the 24-nucleotide Bristol deletion, or other deletions/mutations affecting the furin cleavage site, were not present in our viral stocks.

Vero CCL81 cells were used for the prophylactic and therapeutic assays (ATCC, Manassas, VA). Plaque assays were performed in Vero E6 cells, kindly provided by Vineet Menachery (UTMB, Galveston, TX). The cells were maintained in a 37°C incubator with 5% CO_2. Cells were

propagated utilizing a Dulbecco's Modified Eagle Medium (Gibco, Grand Island, NY) supplemented with 5% fetal bovine serum (FBS) [Atlanta Biologicals, Lawrenceville, GA] and 1% penicillium/streptomycin (Gibco, Grand Island, NY). Maintenance media reduced the FBS to 2% but was otherwise identical. SARS-CoV-2, strain USA_WA1/2020 (Genbank accession MT020880), was provided by the World Reference Center for Emerging Viruses and Arboviruses [26]. All studies utilized a NextGen sequenced Vero passage 4 stock of SARS-CoV-2. Oleandrin (PhytoLab, Vestenbergsgreuth, Germany) was dissolved at a concentration of 1 mg/ml in DMSO (Invitrogen, Eugene, OR).

2.2. LDH Toxicity assay

Plates (96-well plate format) were seeded with 2×10^4 Vero CCL81 cells in 100 μl growth media and returned to a 37 °C/5% CO_2 incubator overnight. The following day, growth media was removed and replaced with 100 μl maintenance media containing either 1–0.005 μg/ml oleandrin in 0.1–0.0005% DMSO, 0.1–0.0005% DMSO without drug, or untreated media to serve as controls for the maximum and spontaneous release of LDH. All treatments were added to triplicate wells, plates were returned to the 37°C/5% CO_2 incubator. At either 24- or 48-h post-treatment, plates were removed from the incubator and the LDH released into the supernatant was assessed using the CyQUANT LDH toxicity assay (Invitrogen, Eugene, OR) according to the manufacturer's instructions. Absorbance was measured at 490 nm and 680 nm on a Synergy HT plate reader (BioTek, Winooski, VT) with Gen5 data analysis software, vr. 2.05 (BioTek, Winooski, VT).

2.3. In vitro prophylactic and therapeutic studies

In the prophylactic studies, growth media was removed from confluent monolayers of approximately 10^6 Vero CCL81 cells in 6-well plates. The growth media was replaced with 200 μl of maintenance media containing either 1.0 μg/ml, 0.5 μg/ml, 0.1 μg/ml, 0.05 μg/ml, 0.01 μg/ml, 0.005 μg/ml oleandrin, or matched DMSO-only controls. Treated plates were returned to the 37 °C/5% CO_2 incubator for 30 min. After pre-treatment, 1×10^4 SARS-CoV-2 plaque forming units (PFU) in a volume of 200 μl maintenance media were added to all wells, yielding a multiplicity of infection (MOI) of 0.01. The infection was allowed to proceed for one h at 37 °C and 5% CO_2. After infection, cells were gently washed 3 times with DPBS (Sigma, St Louis, MO). Finally, 4 ml of maintenance media containing either oleandrin in DMSO or DMSO-only was added to each well according to the pre-treatment concentrations. Samples were taken 24- and 48-h post-infection. Each concentration and control pair were done in triplicate, and the entire study was repeated, again in triplicate. In the therapeutic studies, the pre-treatment step was eliminated. Vero cells were seeded, infected, washed, and returned to the incubator as before. At either 12- or 24-h post-infection, oleandrin in DMSO or matched DMSO-only controls were spiked into the appropriate wells. The two lowest doses (0.01 μg/ml and 0.005 μg/ml) were not included. Samples from the 12-h post-infection treatment were taken 24- and 48-h post-infection. Samples from the 24-h post-infection treatment were taken at 48 h post-infection. Each dose and control pair were done in triplicate.

2.4. Plaque assay

Vero E6 cells were seeded in 6-well plates (Thermo Scientific, Waltham, MA) to a confluency of approximately 90%. Samples were serially 10-fold diluted in DPBS. Diluted samples were plated onto the cells with a volume of 0.25 ml and left to incubate at 37 °C with 5% CO_2 for 1 h. After incubation, samples were overlaid with a 1:1 mixture of one-part 2X MEM (Gibco, Grand Island, NY) supplemented with 8% FBS and 2% pen/strep, and one part 1.6% LE agarose (Promega, Madison, WI). Plates were incubated for two days at 37 °C at 5% CO_2. Plaques were visualized with neutral red stain (Sigma, St Louis, MO) and a light box.

2.5. Genome copy measurement

To quantify genome copies for the samples, 200 μl of sample was extracted with a 5:1 vol ratio of TRIzol LS (Ambion, Carlsbad, CA), utilizing standard manufacturers protocols and resuspending in 11 μl water. Extracted RNA was tested for SARS-CoV-2 by qRT-PCR following a previously published assay [27]. Briefly, the N gene was amplified using the following primers and probe: forward primer [5'-TAATCAGACAAGGAACTGATTA-3']; reverse primer [5'-CGAAGGTGTGACTTCCATG-3']; and probe [5'-FAMGCAAATTGTGCAATTTGCGG-TAMRA-3']. A 20 μl reaction mixture was prepared using the iTaq Universal probes One-Step kit (BioRad, Hercules, CA), according to manufacturer instructions: A reaction mix (2x: 290 10 μl), iScript reverse transcriptase (0.5 μl), primers (10 μM: 1.0 μl), probe (10 μM: 0.5 μl), extracted RNA (4 μl) and water (3 μl). The RT-qPCR reactions were conducted using the thermocycler StepOnePlus™ Real-Time PCR Systems (Applied Biosystems). Reactions were incubated at 50 °C for 5 min and 95 °C for 20 s followed by 40 cycles at 95 °C for 5 s and 60 °C for 30 s. The positive control RNA sequence (nucleotides 26,044–29,883 of SARS-CoV-2 genome) was provided by Dr. Pei-Yong Shi and used to estimate the RNA copy numbers of N gene in the samples under evaluation.

2.6. Statistical analysis

Matched oleandrin-treated samples and DMSO-only controls had their LDH absorbance, percent cytotoxicity, Log_{10}-transformed infectious and genomic equivalent titers, and raw genome to PFU ratios analyzed *via t* -tests (one per concentration) with Holm's correction for multiple comparisons. Values below the limit of detection were assumed to equal one-half of that value for graphing and statistical purposes. All graphs were generated in Prism version 7.03 (GraphPad, San Diego, CA). All statistical analysis was performed in R vr. 3.6.2.

2.7. Animal ethics statement

Ethics statement - All experimental procedures with golden Syrian hamsters were approved by the Texas Biomedical Research Institute (Texas Biomed) Institutional Animal Care and Use Committee (IACUC, #1732 MU) and conducted under Animal Biosafety Level 2 (ABSL2).

2.8. Animals

For the determination of safety, four-week-old female golden Syrian hamsters were purchased from Charles River Laboratories (Wilmington, MA). Each experimental group had 5 hamsters. Hamsters were housed in microisolator cages (Texas Biomed ABSL2) and were provided sterile water and chow *ad libitum* and acclimatized for at least one week prior to experimental manipulation. Baseline body weights were measured before treatments with oleander extract or vehicle control commenced.

For the determination of efficacy, four-week-old female golden Syrian hamsters were purchased from Charles River Laboratories (Wilmington, MA.). Each experimental group had 5 hamsters per time point. Hamsters were housed in micro-isolator cages in the ABSL3 setup. Hamsters were provided sterile water and chow *ad libitum* and acclimatized for at least one week prior to experimental manipulation. Baseline body weights were measured before oleandrin treatment was started and was continued during the study.

2.9. In vivo treatment regimen

Prompted by the significant *in vitro* antiviral efficacy of the purified oleandrin, we conducted in-depth safety/toxicity analyses of a model solution of PBI-06150 containing 1.3, 13 or 130 μg of oleandrin (measured by LC/MS/MS) per ml of vehicle (40% ethanol in water) in golden Syrian hamsters, a relevant animal model of SARS-CoV-2

infection. Vehicle and PBI-06150 solutions (containing 1.3, 13 or 130 μg oleandrin/ml) were stored at 4 °C. Before using, solutions were determined to be homogeneous. Different groups of animals were dosed with 25 μl of extract containing each of the different oleandrin concentrations, or vehicle control, by the sublingual route once daily by using sterile pipette tips for 7 consecutive days. Treatment was stopped after the 7th dose. All the hamsters were monitored daily for morbidity (body weight loss) and mortality (survival) changes for 21 days post-treatment. A subset of hamsters (n = 5) from each experimental group was euthanized at days 7 and 21 post-treatment to assess if treatment caused any acute or chronic cytotoxic effects. Lungs, brain, and heart tissues from treated hamsters were collected and fixed in 10% neutral buffered formalin for histopathologic examination. Serum from blood samples collected from the animals were aliquoted and stored at − 80 °C until further use.

We also conducted *in vivo* studies in the infected hamsters. Vehicle and PBI-06150-containing solutions (described above) were stored at 4 °C. Before using, solutions were homogeneously mixed and 25 μl of oleander extract solution or vehicle were sublingually administered once a day into hamsters by using sterile pipette tips for 5 consecutive days prior to SARS-CoV-2 infection. One-day post last dose of treatment, hamsters were infected intranasally (i.n.) with 2×10^5 PFU of SARS-CoV-2 P6 in a final volume of 100 μl following isoflurane sedation. Hamsters (n = 5/time-point) from vehicle and oleander extract treated groups were euthanized on 1-, 2-, 3-, 4- and 7-days post-infection (DPI). Nasal turbinates were collected, homogenized and aliquots were stored in − 80 °C.

PBI-06150 was obtained by a proprietary process involving a combination of extractions of *Nerium oleander* leaves, the same starting material used for the preparation of PBI-05204. The composition of PBI-06150 is proprietary; however, it is an extract containing a defined concentration of oleandrin along with other compounds found in PBI-05204 that have previously been described [24]. The contents of the extract are provided as a solution in ethanol, whereas, PBI-05204 is provided as supercritical CO_2 semi-solid paste.

2.10. Histopathology

Formalin-fixed tissues (lung, brain, and heart) were embedded in paraffin blocks and used to make 5 μm thick sections. Hematoxylin and Eosin (H&E) stained tissues were examined by a veterinary pathologist in a blinded manner. An Olympus BX50 microscope was used to take pictures of the H&E-stained sections.

2.11. Hepatic enzyme levels and activities

Hamster ALP (MBS011057) and ALT (MBS011423) quantitative sandwich ELISA kits were procured from MyBioSource, Inc. (San Diego, CA) and used to measure ALP and ALT levels, respectively, in serum as per the manufacturer's instructions. Colorimetric assays (p-nitrophenyl and pyruvate based) were used to measure ALP (ab83369, Abcam, Cambridge, MA) and ALT (ab105134) activities, respectively, in serum and calculated as per the manufacturer's instructions. All plates were read in a microplate reader form Molecular Devices (San Jose, CA).

2.12. Virus quantitation in nasal turbinates

Vero E6 cells were seeded at a density of 2×10^5 cells/well in flat bottom 24-well tissue culture plates. The following day, media was removed and replaced with 100 μl of ten-fold serial dilutions of the nasal turbinate homogenate. Virus was adsorbed for 1 h at 37 °C in a humidified 5% CO_2 incubator. After viral adsorption, post-infection media containing 0.9% agarose overlay (Sigma-Aldrich) was added and cells were incubated in a humidified 5% CO_2 incubator at 37 °C for 48 h. After 48 h, plates were inactivated in 10% neutral buffered formalin (Thermo-Fisher Scientific) for 12 h. For immunostaining, cells were washed three times with DPBS and permeabilized with 0.5% Triton X-100 for 10 min at room temperature. Cells were immunostained with 1 μg/ml of a SARS-CoV-1/-2 nucleocapsid protein (NP) cross-reactive monoclonal antibody (Mab; Sigma-Aldrich) 1C7, diluted in 1% BSA for 1 h at 37 °C. After incubation with the primary NP MAb, cells were washed three times with PBS, and developed with the Vectastain ABC kit and DAB Peroxidase Substrate kit (Vector 580 Laboratory, Inc., CA, USA) according to manufacturers' instructions. Viral determinations were conducted and viral titers were calculated by number of counted plaques for a given dilution and results were presented as PFU/ml.

3. Results

3.1. In vitro toxicity of oleandrin

A range of oleandrin concentrations (1 μg/ml to 0.005 μg/ml) was selected based on previous studies that evaluated inhibition of other viral infections [21,22], as well as studies of its role as an effective anticancer cardiac glycoside [28]. Because oleandrin was dissolved in DMSO, negative controls containing equal concentrations of DMSO in the absence of oleandrin were also tested. First, a lactate dehydrogenase release assay for cytotoxicity was performed to establish the suitability of the intended experimental system. Overall, oleandrin was well tolerated by the highly SARS-CoV-2-susceptible Vero cell line (Fig. 1). At 24 h post-treatment, no significant differences were observed between oleandrin and the DMSO controls (Fig. 1A). By 48 h post-treatment, significant differences were observed (Fig. 1B). However, absolute differences were relatively modest compared to the maximum cytotoxicity of Triton-X100, which was included as an assay control. The highest cytotoxicity of oleandrin was observed at the 0.1 μg/ml concentration, with an increase of 1.86% cytotoxicity in the DMSO control to 6.88% in the oleandrin-treated wells for a drug-dependent difference of 5.02%. All other oleandrin concentrations caused ≥ 2% overall cytotoxicity.

3.2. In vitro prophylactic efficacy

To assess the prophylactic potential of oleandrin in the context of SARS-CoV-2 infection, Vero CCL81 cells, shown previously to be highly susceptible [25], were pre-treated with oleandrin or DMSO-carrier controls for 30 min prior to infection. SARS-CoV-2, strain USA_WA1/2020 was used to infect the cells, and post-infection culture medium was also supplemented with either oleandrin in DMSO, or DMSO alone. Tissue culture supernatant samples were collected at 24- and 48 h post-infection, at which point the experiments were terminated due to the onset of substantial viral-associated cytopathic effects (CPE) in the DMSO controls.

In the absence of oleandrin, SARS-CoV-2 reached approximately 6 $\log_{10}$ PFU/ml titers by the 24-h timepoint and maintained that titer at the later timepoint (Fig. 2A, B). DMSO controls all reached similar titers, with no dose-dependent trend observed. The four highest concentrations of oleandrin (1.0 μg/ml to 0.05 μg/ml) significantly reduced the production of infectious SARS-CoV-2. Oleandrin concentrations at 1.0 μg/ml to 0.5 μg/ml reduced SARS-CoV-2 titers by more than 4 $\log^{10}$ PFU/ml, which consistently remained either at or below the limit of detection for this assay. This corresponded to a nearly complete reduction in infectious SARS-CoV-2 titer for the 0.05 μg/ml through 1.0 μg/ml oleandrin concentrations (Fig. 2C). The 0.1 μg/ml oleandrin dose resulted in a greater than 3000-fold reduction, and the 0.05 μg/ml concentration resulted in an 800-fold reduction. However, 0.01 μg/ml and 0.005 μg/ml concentrations had no significant effect on SARS-CoV-2 production. At the 48 h timepoint, the DMSO controls maintained approximately the same titer observed earlier, while oleandrin concentrations ranging from 1.0 μg/ml to 0.05 μg/ml maintained their significant reductions in SARS-CoV-2 titers. Interestingly, the 0.01 μg/ml dose, which had no significant effect compared to its DMSO control at 24 h post-infection, did result in a statistically significant reduction in viral titers at 48 h

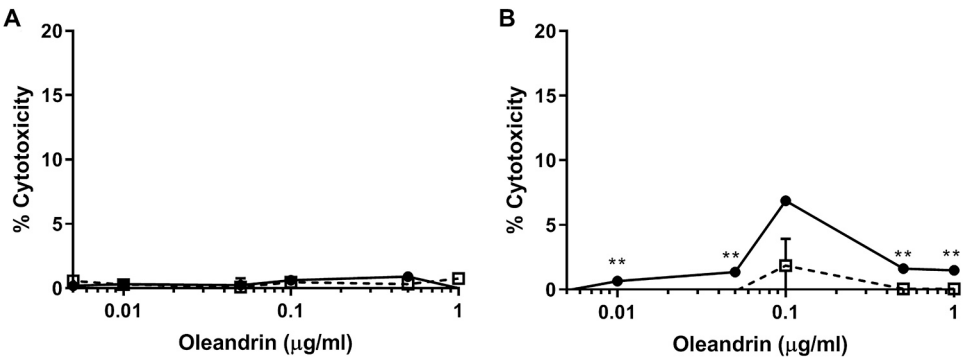

Fig. 1. Oleandrin is well tolerated by Vero cells. Release of LDH was measured as a proxy for cytotoxicity potentially induced by varying concentrations of oleandrin and DMSO-matched controls. LDH levels released in the supernatant were measured at 24 h (A) and 48 h (B) after the addition of oleandrin. Absolute absorbance values were normalized to a percent cytotoxicity (A and B), with the spontaneous release of LDH in untreated cells set as 0 and the maximum release of LDH in Triton-X100-treated cells set as 100. Symbols (-•-, oleandrin + DMSO; -□-, DMSO control) represent the mean, error bars represent standard deviations. Oleandrin-treated cells and their DMSO-matched controls were compared *via t* -tests with Holms correction for multiple comparisons to test for any drug associated cytotoxicity. ** = $p < 0.01$.

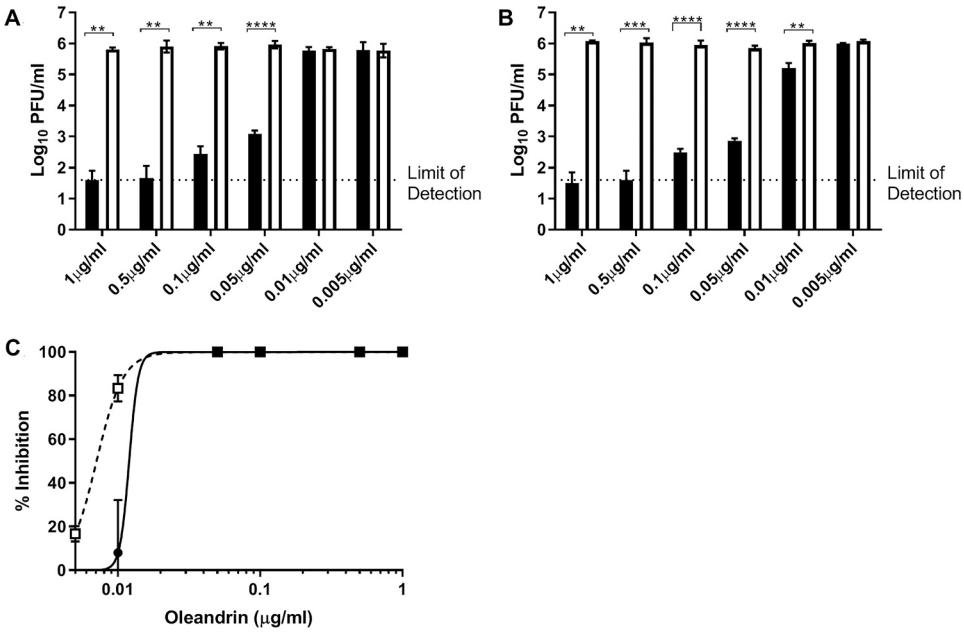

Fig. 2. Oleandrin pre-treatment reduces SARS-CoV-2 infectious titers when added prior to infection. Various concentrations of oleandrin or DMSO-matched controls were added to Vero CCL81 cells 30 min prior to infection (MOI = 0.01) and were maintained after infection as well (A, B; closed bars). Supernatants were collected 24 h (A) and 48 h (B) after infection. Infectious SARS-CoV-2 titers were quantified *via* plaque assay, and the percent viral inhibition in oleandrin-treated samples *vs.* their corresponding DMSO-matched controls were calculated (C). Relative inhibition of viral titers is shown (C). Data from 24 h incubation (open symbol) and 48 h incubation with oleandrin are shown. Data are shown from a single representative experiment conducted in triplicate. Bar heights represent the mean, error bars represent the standard deviation. Oleandrin-treated samples (A, B: closed bars) and DMSO-matched controls (open bars) were compared *via t* -tests, with a Holms correction for multiple comparisons. ** = $p < 0.01$, *** = $p < 0.001$, **** = $p < 0.0001$.

post infection ($p < 0.01$; Fig. 2B). This trend of a greater drug-induced reduction observed at 48 h as compared to 24 h was consistent at the higher concentrations of oleandrin as well (Fig. 2C). At 1.0 μg/ml, the effect increased to 18,822-fold reduction at 24 h to 44,000-fold reduction at 48 h, and at 0.5 μg/ml the effect increased from 23,704-fold to 32,278-fold. Reductions observed for 0.1 μg/ml and 0.05 μg/ml remained similar at 24- and 48 h post-infection. The 0.01 μg/ml concentration of oleandrin decreased SARS-CoV-2 titers by 6.3-fold. The increased prophylactic efficacy of oleandrin over time (24 *vs.* 48 h) was reflected in its EC_{50} values, calculated at 11.98 ng/ml at 24 h post-infection and 7.07 ng/ml at 48 h post-infection. The study was repeated in its entirety and confirmed the previous finding.

3.3. Genomic equivalents and genome to PFU ratios

Cardiac glycosides have been shown to inhibit the formation of infectious HIV particles through reduction of the virus envelope [21]. To determine whether the inhibition of oleandrin on SARS-CoV-2 was at the level of total or infectious to non-infectious ratio particle production, RNA was extracted from the cell culture supernatants of the prophylactic study and genomic equivalents were quantified *via* RT-qPCR (Fig. 3). The antiviral effect of oleandrin, initially observed *via* infectious assay, was confirmed at the level of genome equivalents. At 24 h post-infection, oleandrin significantly decreased SARS-CoV-2 genome copies in the supernatant at the four highest concentrations (Fig. 3A). By 48 h post-infection, all but the lowest concentration resulted in significant reductions in SARS-CoV-2 genome copies (Fig. 3B), confirming results observed from the infectious assay in which the 0.01 μg/ml concentration gained efficacy as the infection proceeded. Genome to infectious virus particle PFU ratios were also calculated (Fig. 3C, D). While differences between the oleandrin-treated samples and their DMSO controls were not significant, there were several interesting trends. First, at both 24- and 48 h post-infection the higher, more efficacious concentrations of oleandrin had higher genome to PFU ratios than their DMSO controls (Fig. 3C, D). Second, this effect was more pronounced at 48 h rather than at 24 h post-infection, suggesting that oleandrin may have reduced the infectivity of SARS-CoV-2 viral progeny.

3.4. In vitro therapeutic efficacy

Also tested was the effect of oleandrin when added post SARS-CoV-2 infection. The 4 higher concentrations of 1.0 μg/ml to 0.05 μg/ml were added at either 12- or 24 h post-infection. DMSO-matched controls were

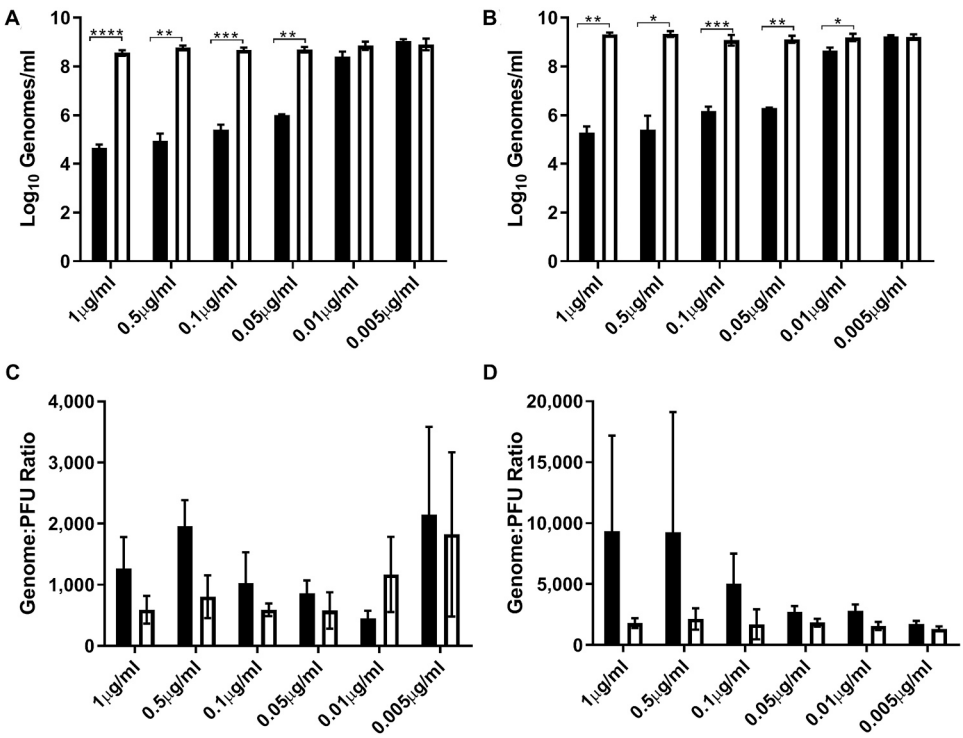

Fig. 3. Oleandrin pre-treatment reduces SARS-CoV-2 genome copies when added prior to infection. Various concentrations of oleandrin or DMSO-matched controls were added to Vero cells 30 min prior to infection (MOI = 0.01) and were maintained after infection as well. Supernatants were collected 24 h (A and C) and 48 h (B and D) after infection. SARS-CoV-2 genome copies were quantified *via* qRT-PCR (A and B), and the genome to PFU ratios were calculated using the previous obtained infectious titers (C and D). Data shown from a single representative experiment conducted in triplicate. Bar heights represent the mean, error bars represent the standard deviation. Oleandrin-treated samples (solid bars) and DMSO-matched controls (open bars) were compared *via t* -tests, with a Holms correction for multiple comparisons. * = $p < 0.05$, ** = $p < 0.01$, *** = $p < 0.001$, **** = $p < 0.0001$.

again included. Samples were harvested from the 12 h treatment at both 24- and 48 h post-infection (Fig. 4A-D). At 24 h post-infection, oleandrin reduced SARS-CoV-2 titers by approximately 10-fold (Fig. 4B), despite a short treatment time of only 12 h. Importantly, by 48 h post-infection, the effect became more pronounced both in terms of the titer reduction and absolute titers. The highest concentration of oleandrin resulted in a greater than 1000-fold reduction in infectious SARS-CoV-2 titer, with the 0.5 μg/ml and 0.1 μg/ml concentrations causing greater than 100-fold reductions, and the 0.05 μg/ml concentration resulting in a 78-fold reduction (Fig. 4D). Oleandrin maintained its therapeutic effect even when added at 24 h post-infection (Fig. 4E, F), a timepoint at which extensive SARS-CoV-2 replication has already occurred. The 24 h treatment resulted in a 5–10-fold reduction in titers measured at 48 h post-infection, similar to the impact of 12 h treatment measured at 24 h post-infection. Due to the viral-induced CPE in the DMSO-only treated wells, testing beyond 48 h to determine the extended therapeutic

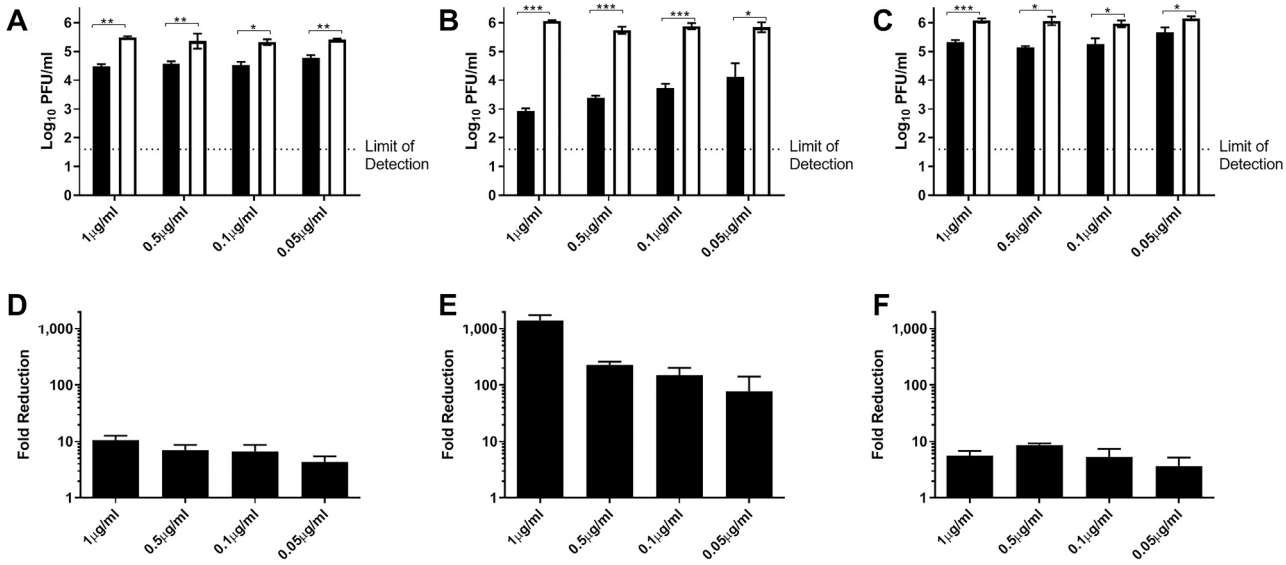

Fig. 4. Oleandrin reduces SARS-CoV-2 infectious titers when added after infection. Various concentrations of oleandrin or DMSO-matched controls were added to Vero CCL81 cells either 12 h (A, B, D, and E) or 24 h (C and F) after infection (MOI = 0.01). Supernatants were collected 24 h (A and D) after infection from the samples previously drugged at 12 h post-infection. Supernatants were also collected 48 h after infection from both the samples previously drugged at 12 h post-infection (B and E) and at 24 h post-infection (C and F). Infectious SARS-CoV-2 titers were quantified *via* plaque assay (A, B, and C), and the fold reduction in oleandrin-treated samples *vs.* their corresponding DMSO-matched controls were calculated (D, E, and F). Data shown from a single representative experiment conducted in triplicate. Bar heights represent the mean, error bars represent the standard deviation. Oleandrin treated samples (closed bars) and DMSO-matched controls (open bars) were compared *via t* -tests, with a Holms correction for multiple comparisons * = $p < 0.05$, ** = $p < 0.01$, *** = $p < 0.001$.

efficacy was not performed.

3.5. Animal body weight data analysis

Before administration of the first oleander extract or vehicle treatment (day 0), hamsters were weighed daily until the end of the study (day 21 post-treatment). At no point during treatment with extract of vehicle control did the hamsters show any signs of morbidity. Under all conditions, hamsters continued gaining weight (Fig. 5A). Even animals treated with the highest oleandrin content in the extracts (130 μg oleandrin/ml) did not show any adverse body weight effects (Fig. 5A). All hamsters survived the oleander extract treatments (Fig. 5B).

3.6. In vivo histopathology

H&E-stained sections of lungs, heart and brain from the vehicle and oleander extract treated hamsters were examined for histologic lesions. The lungs of vehicle and all oleander extract treated groups showed similar lesions of minimal interstitial, alveolar and perivascular inflammation (infiltration of small numbers of macrophages, neutrophils and few lymphocytes and plasma cells) with minimal hemorrhage at both days 7 and 21 post-treatment (Fig. 6A to D, micrographs a-g). Rarely, in all experimental groups, alveolar septa, bronchi and bronchioles were lined by syncytial cells (2–4 nuclei) (Fig. 6A to D, micrographs d and e). However, no differences in type or severity of inflammation were observed between any of the groups. All brain sections across the four groups showed no significant histopathology and had similar histologic lesions with mild meningeal hemorrhage (presumed collection artifact) and occasional slightly shrunken, basophilic neurons with pyknotic nucleus (presumed artifact; data not shown). Similarly, hearts from all four groups showed no significant histopathology. There was mild myocardial hemorrhage in a few animals across all groups which was not associated with any inflammation or necrosis (presumed to be the result of postmortem intracardiac blood collection).

3.7. In vivo ALP and ALT serum enzyme determination

Physiological parameters for oleander extract induced hepatic damage were determined by measurement of serum ALP and ALT levels on days 7 and 21 post-treatment (Fig. 7). Serum levels of ALP and ALT were extremely low or below the limit of detection (0.625–20 ng/ml and 0.25–8 ng/ml, respectively) in all experimental groups studied. Moreover, similar to histopathology results, there were no differences in ALP (Fig. 7A, B) and ALT (Fig. 7C, D) levels between the vehicle control and PBI-06150 treated groups at various oleandrin concentrations administered to hamsters. ALP and ALT activities were also measured to confirm that oleandrin within the extracts did not cause any hepatic cytotoxicity (Fig. 8). At days 7 (Fig. 8A, C) and 21 (Fig. 8B, D) post-treatment, ALP and ALT activities showed no significant increase in serum of hamsters treated with PBI-06150 as compared to vehicle treated hamsters. There was no dose dependent effect detected in the PBI-06150 treated hamsters.

3.8. In vivo therapeutic efficacy in hamster model

To determine the prophylactic effect of PBI-06150 (5 days pre-treatment) on SARS-CoV-2 infection, hamsters were sacrificed at 1, 2, 3, 4 and 7 DPI (days post infection) and viral loads in nasal turbinates were determined. Viral load in nasal turbinates of both vehicle and PBI-06150-treated hamsters was about 10^4 to 10^5 PFU/ml at 1 and 2 DPI (Fig. 9) However, at 3 DPI viral loads in nasal turbinates of PBI-06150-treated hamsters were below the limit of detection (10 PFU/ml), whereas in the vehicle treated group, 3 out of 5 hamsters showed viral titers at 1.8×10^3 PFU/ml. The viral load was below the detection limit in the remaining 2 hamsters. Nasal turbinate viral loads in both hamster's groups cleared at 4 DPI (Fig. 9).

4. Discussion

The emergency COVID-19 pandemic situation calls for rapid screening of potential therapeutic or prophylactic drugs already shown in prior clinical trials to be safely tolerated. Previously reported was the safe use of a defined extract of *N. oleander* PBI-05204 in clinical Phase I and II trials in patients with advanced malignant disease [17,18]. Here, the prophylactic and therapeutic *in vitro* efficacy of oleandrin, a cardiac glycoside extracted from the *N. oleander* plant, against SARS-CoV-2 was tested. As in previous studies with other viruses, oleandrin exhibited potent antiviral activity against SARS-CoV-2. Treatment of Vero cells starting at 30 min prior to the 48 h culture period with as little as 0.05 μg/ml resulted in a significant, 800-fold reduction in virus production, and at 0.1 μg/ml oleandrin treatment resulted in a greater than 3000-fold reduction in infectious virus as well as a similar reduction in viral RNA copies. The EC_{50} values were 11.98 ng/ml when virus output was measured at 24 h post-infection, and 7.07 ng/ml measured at 48 h post-infection. Therapeutic (post-infection) treatment up to 24 h after infection of Vero cells also reduced viral titers, with the 0.5 μg/ml and 0.1 μg/ml doses causing greater than 100-fold reductions measured at 48 h, and the 0.05 μg/ml dose resulting in a 78-fold reduction.

The pharmacology of oleandrin has been a subject of expanded examination during the past 20 years [28]. Its most recognized activity is inhibition of Na, K-ATPase through blockade of ATP binding sites. Other membrane-positioned enzymes requiring ATP include ACE-2 which has now been shown to be an entry receptor for SARS-CoV-2 [29]. The potential role of oleandrin as an active principal ingredient in the botanical drug (PBI-05204) designed to treat malignant disease has been reported [14–16, 28]. The Phase I clinical trial of PBI-05204, for example, included measurement of C_{max} and $t_{1/2}$ calculations for oleandrin after oral administration to cancer patients. The delayed oral administration

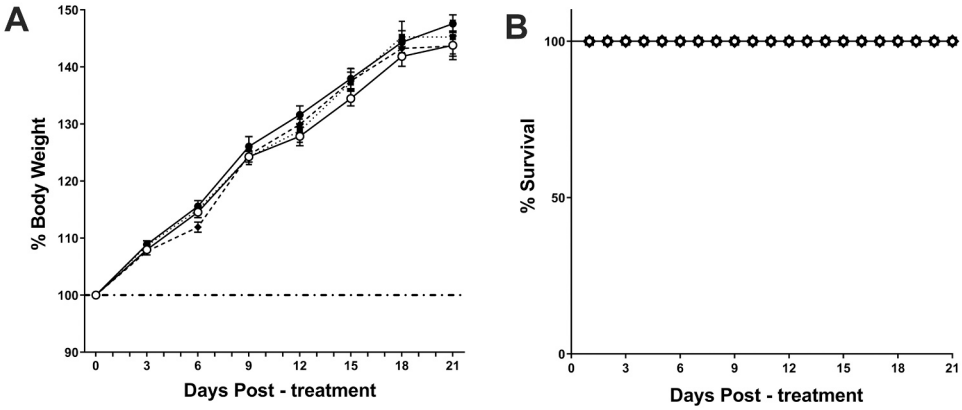

Fig. 5. Body weight and survival of golden Syrian hamsters treated with vehicle or the indicated concentrations of oleander extract. Body weight (A) and survival (B) data from days 0–7 were obtained from 10 hamsters in each experimental group, whereas 5 hamsters in each group were used from days 8–21. Data presented as Mean ± SEM from animals treated with control vehicle (-○-), oleander extract (oleandrin 1.3 μg/ml: -◆-); oleander extract (oleandrin 13 μg/ml: -●-); and oleander extract (oleandrin 130 μg/ml: -■-).

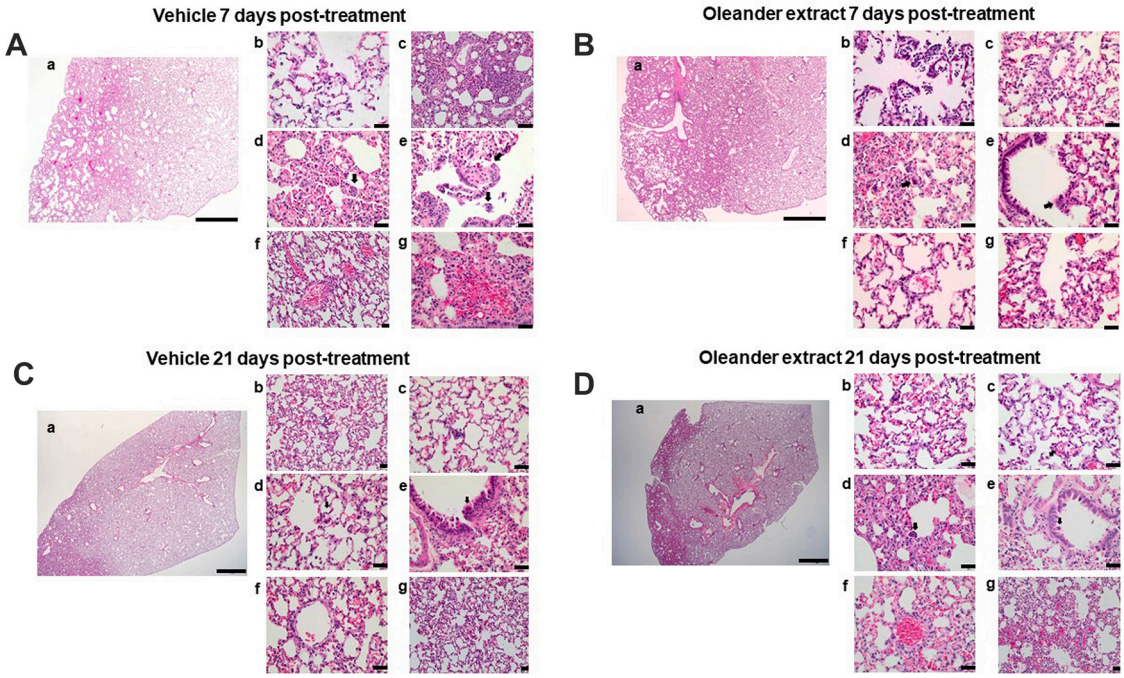

Fig. 6. Histopathology analysis of golden Syrian Hamsters treated with oleander extract. Representative image of H&E-stained lung section of vehicle (A and C) and oleander extract [oleandrin 130 μg/ml] (B and D) treated hamsters at days 7 (A and B) and 21 (C and D) post-treatment: (a) lung, (b) alveolar space inflammation, (c) alveolar interstitial inflammation, (d) alveolar septa syncytia, (e) bronchiolar syncytia, (f) perivascular inflammation, and (g) hemorrhage images are shown. Scale bar from micrograph a = 1 mm; b to g = 50 μm.

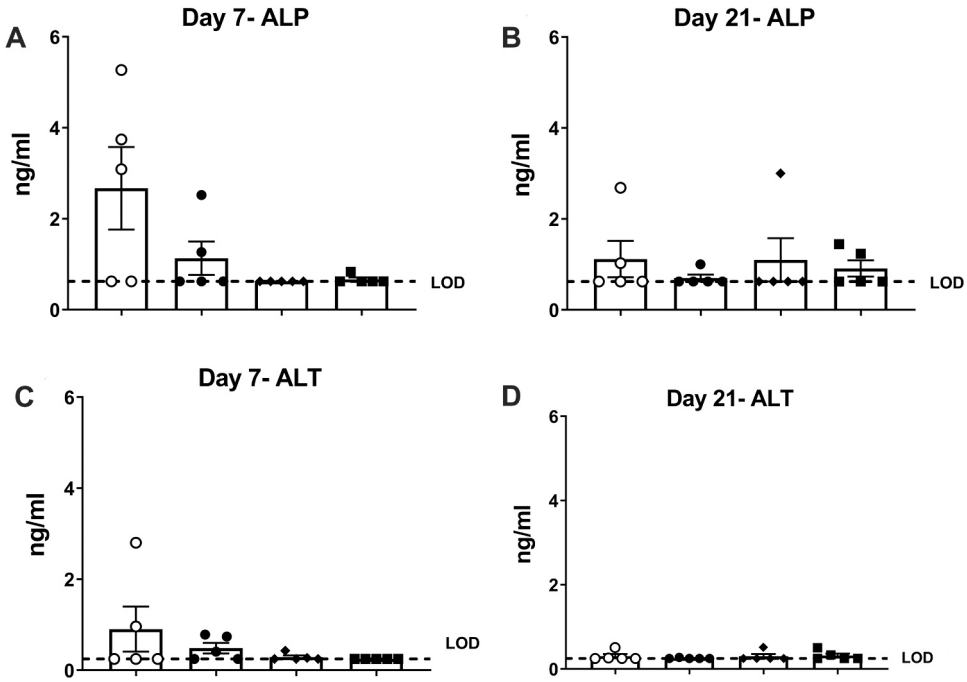

Fig. 7. Serum alkaline phosphatase (ALP) and alanine transaminase (ALT) levels at days 7 (A and C) and 21 (B and D) post-treatment with oleander extract (oleandrin 130 μg/ml). Data are presented as Mean ± SEM from animals treated with control vehicle (-O-), PBI-06150 (oleander extract; oleandrin 1.3 μg/ml: -●-), PBI-06150 (oleandrin 13 μg/ml: -◆-) and PBI-06150 (oleandrin 130 μg/ml: -■-).

of this candidate drug achieved plasma concentrations of 2–4 ng oleandrin/ml, without significant adverse effects, at a dose determined to be appropriate for Phase II clinical studies. The measured half-life was variable at 8–13 h, indicating that multiple daily administrations may be optimal for maximum benefit [17]. Our unpublished studies have shown that sublingual administration of oleandrin as an extract of *N. oleander* offers facile, safe and rapid plasma concentrations of oleandrin that surpass those achieved after oral administration, on a dose-equivalent basis. This is likely attributable to the fact that oral administration of oleandrin may result in cleavage of this molecule in liver tissue to the much less active metabolite oleandrigenin, whereas sublingual administration is known to avoid first-pass metabolism.

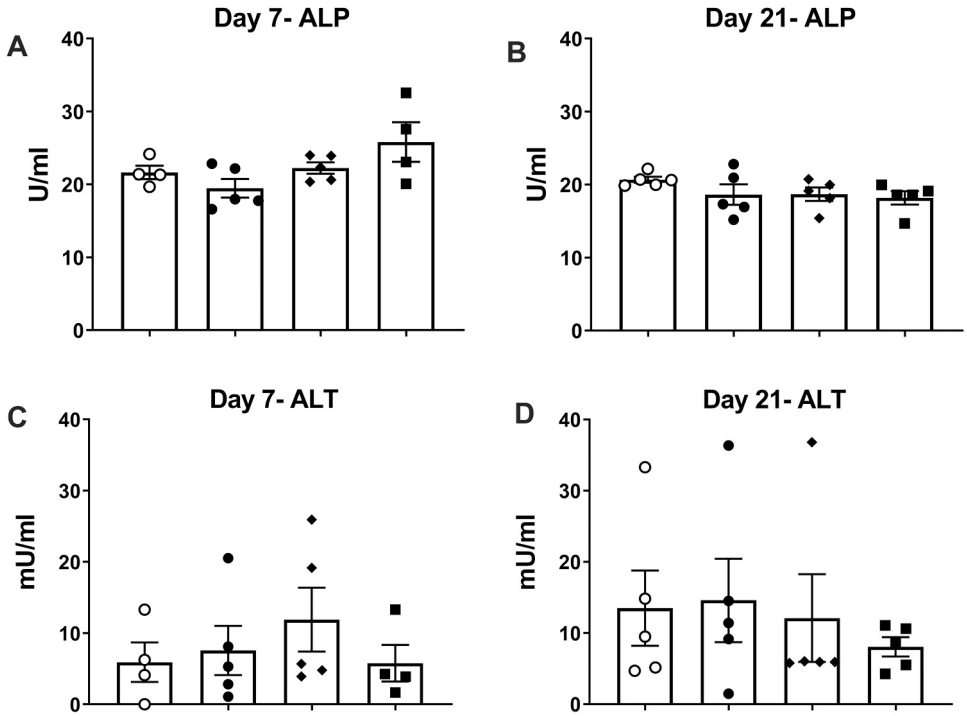

Fig. 8. Serum ALP and alanine transaminase (ALT) activities at days 7 (A & C) and 21 (B & D) post-treatment with oleander extract. Data are presented as Mean ± SEM from animals treated with control vehicle (-O-), PBI-06150 (oleandrin 1.3 μg/ml: -●-), PBI-06150 (oleandrin 13 μg/ml: -◆-) and PBI-06150 (oleandrin 130 μg/ml:-■-).

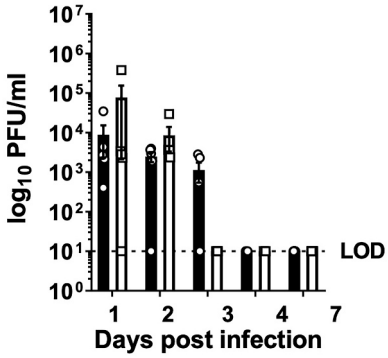

Fig. 9. Replication of SARS-CoV-2 in the upper respiratory tract of hamsters treated with oleander extract. Viral titers in the nasal turbinates of infected hamsters are represented as mean values calculated from n = 5 hamsters in each group/day. LOD: Limit of detection. Open circles (-O-) represent individual data points and solid bars (-- ▒ --) represent mean + SEM values from vehicle treated animals. Open squares (-□-) represent individual data points and open bars (-- ▯ --) represent mean + SEM data from PBI-06150 (oleandrin 130 μg/ml) treated animals.

Prior preclinical research demonstrated that oleandrin, in contrast to other cardiac glycosides such as digoxin, readily crosses the blood-brain barrier, where it induces beneficial effects such induction of brain derived neurotrophic factor (BDNF) and induction of nuclear factor erythroid 2-related factor 2 (Nrf-2), providing antioxidant activities [30]. Given the poorly understood neurological manifestations presenting in some COVID-19 patients [31,32], oleandrin may therefore be of some benefit in preventing virus-associated neurological disease. Further studies are needed including animal models that reproduce what are known as 'COVID-19-long related' neurological signs.

Oleandrin and extracts containing this molecule have also been shown to produce a strong anti-inflammatory response, which may be of benefit in preventing hyper-inflammatory responses to infection with SARS-CoV-2 [33]. Here it is shown that low concentrations of oleandrin exhibit strong antiviral activity against SARS-CoV-2. Thus, considering the beneficial anti-inflammatory activity of *N. oleander* extracts combined with the suggestion that oleandrin might protect against neurological deficits, PBI-06150, which is formulated for sublingual administration, was developed (Phoenix Biotechnology, Inc., San Antonio, TX) and is intended for an exploration of relative efficacy in an appropriate pilot human clinical study. Additional studies are clearly needed to define the mechanism of oleandrin's antiviral activity. Several steps in viral replication could be affected including entry/fusion, lipid metabolism related to budding, formation of replication complexes, secretory pathway function and effects on SARS-CoV-2 protein processing, *etc.* Also, *in vivo* studies using validated animal models such as K18 human angiotensin converting enzyme 2 (hACE2) transgenic mouse [34], gold Syrian hamster [23,35], ferret [36] and/or nonhuman primates [37] should be conducted to specifically test the preventive and/or therapeutic efficacy potential of oleandrin and extracts that contain this molecule against SARS-CoV-2 infection *in vivo*. It would also be of interest to examine oleandrin for its relative ability to inhibit other enveloped viruses such as closely related SARS-CoV and MERS-CoV, or other respiratory viruses (*e.g.*, influenza). Overall, the data demonstrate that oleandrin, either in pure form or as part of an extract obtained from *Nerium oleander*, has potent anti-SARS-CoV-2 activity *in vitro*, both when administered before or after infection. Care must be taken, however, when inferring potential human or animal therapeutic benefits from *in vitro* antiviral effects.

Following the demonstration of potent *in vitro* activity of oleandrin, it is critical to demonstrate the safety of the proposed therapeutic product PBI-06150 containing this unique molecule in a relevant COVID-19 animal model. The safety of PBI-05204, a closely related extract of *N. oleander*, has previously been shown in humans and animals [17, 18, 24]. The golden Syrian hamster has recently been reported as a physiological small animal model to study the transmission, pathogenesis, treatment, and vaccination against SARS-CoV-2 [23,35]. Our results

indicate that daily single treatment with PBI-06150 (containing 1.3, 13, or 130 μg/ml concentrations of oleandrin) for 7 consecutive days in hamsters showed no overtly detectable signs of toxicity. All PBI-06150-treated hamsters continued to gain weight without any morbidity or mortality. The magnitude of weight gain in PBI-06150-treated hamsters was comparable to those observed in the vehicle control group. Moreover, histopathology analysis of lungs, brain (data not shown) and heart (data not shown) from PBI-06150-treated hamsters showed no signs of cytotoxicity. Both vehicle control and PBI-06150 treatments showed mild to minimal inflammation in hamster's lungs. The small extent of inflammation noted in the lung was presumed to be a background lesion independent of the treatments. Serum ALP and ALT levels and activities were similar in all oleander extract treated hamster groups and comparable to vehicle treated control animals, suggesting no or minimal hepatic toxicity.

The hamster model was also used to evaluate the *in vivo* efficacy of the extract toward treating SARS-CoV-2 infection. It is important to note that this viral infection is not lethal to these hamsters and instead merely results in a temporary weight loss for a period of about four days [35]. After that period, the animals begin to exhibit normal weight gain; accordingly, any antiviral efficacy must be found prior to day 4 DPI. Infected hamsters were sublingually administered vehicle or vehicle with PBI-05204 to the buccal cavity to mimic buccal or sublingual administration, rather than administration by oral gavage, which mimics peroral administration. The period of time the animals kept the solution in the buccal cavity was not determined, so it is possible some of the solution was swallowed shortly after administration and some was retained in the buccal cavity. The viral titer of the nasal turbinates, obtained from euthanized hamsters, was determined on tissue collected 1, 2, 3, 4, and 7 DPI. The results (Fig. 9) demonstrate that three out of five of the vehicle control group exhibited a viral load in the nasal turbinates at day 3 and no viral load in the nasal turbinates at about day 4; however, none of the hamsters in the PBI-06150-treated group exhibited a viral load in the nasal turbinates at day 3 or later. The results were statistically significant and provide initial evidence for the efficacy of the oleander extract in treating SARS-CoV-2 infection *in vivo*. These results are of great interest, because it is widely believed that the primary points of entry of the virus into humans is through the nose and mouth; accordingly, a product that reduces the viral load in the nasal turbinates might prove to be a significant contribution toward the prevention or treatment of COVID-19 infection.

Having demonstrated both highly significant *in vitro* antiviral activity as well as *in vivo* safety and antiviral activity of PBI-06150 in the golden Syrian hamster, we will next evaluate this extract in another model for SARS-CoV-2 infected animals. These data will be reported in a follow up study. The list of specific enveloped viruses, now including SARS-CoV-2, against which oleandrin and extracts containing this molecule have been shown to be effective continues to expand [20]. As such, consideration of this re-purposed cardenolide as a safe and effective antiviral agent with its unusual ability to reduce progeny viral infectivity should be given serious further consideration.

Conflict of interest statement

RAN is Chief Science Officer of Phoenix Biotechnology Inc. KJS is a paid consultant with Phoenix Biotechnology Inc. RM is a Director of Phoenix Biotechnology, Inc.

Acknowledgements

This research was supported in part by NIH grant R24 AI120942 to SCW. We thank Natalie Thornburg (Centers 305 for Disease Control and Prevention, Atlanta, GA, USA) and the World Reference Center for Emerging Viruses and Arboviruses for providing the SARS-CoV-2 USA_WA1/2020 isolate. Research was also supported by Phoenix Biotechnology, Inc. Experimental design, conduct of the experiments, and interpretation of the data were the independent products of scientists at University of Texas Medical Branch (Galveston) and Texas Biomedical Research Institute with consulting comments from R. A. Newman, PhD, and K. Jagannadha Sastry, PhD. The authors thank Bev Newman, M.S., R.N. for graphic art support.

References

[1] T. Burki, Outbreak of coronavirus disease 2019, Lancet Infect. Dis. 20 (2020) 292–293.
[2] World Health Organization, COVID-19 Weekly Epidemiological Update, Retrieved from http://www.who.int, 19 JAN 2021.
[3] A.M.H. Antommaria, T.S. Gibb, A.L. McGuire, P.R. Wolpe, M.K. Wynia, M. K. Applewhite, A. Caplan, D.S. Diekema, D.M. Hester, L.S. Lehmann, R. McLeod-Sordjan, T. Schiff, H.K. Tabor, S.E. Wieten, J.T. Eberl, Ventilator triage policies during the COVID-19 pandemic at U.S. hospitals associated with members of the association of bioethics program directors, Ann. Intern. Med. 173 (3) (2020) 188–194.
[4] K.L. Flanagan, E. Best, N.W. Crawford, M. Giles, A. Koirala, K. Macartney, F. Russell, B.W. Teh, S.C. Wen, Progress and pitfalls in the quest for effective SARS-CoV-2 (COVID-19) vaccines, Front. Immunol. 11 (2020), 579250.
[5] J.H. Beigel, K.M. Tomashek, L.E. Dodd, A.K. Mehta, B.S. Zingman, A.C. Kalil, E. Hohmann, H.Y. Chu, A. Luetkemeyer, S. Kline, D. Lopez de Castilla, R. W. Finberg, K. Dierberg, V. Tapson, L. Hsieh, T.F. Patterson, R. Paredes, D. A. Sweeney, W.R. Short, G. Touloumi, D.C. Lye, N. Ohmagari, M.D. Oh, G.M. Ruiz-Palacios, T. Benfield, G. Fatkenheuer, M.G. Kortepeter, R.L. Atmar, C.B. Creech, J. Lundgren, A.G. Babiker, S. Pett, J.D. Neaton, T.H. Burgess, T. Bonnett, M. Green, M. Makowski, A. Osinusi, S. Nayak, H.C. Lane, ACTT-1 study group members, remdesivir for the treatment of covid-19 - final report, N. Engl. J. Med. 383 (19) (2020) 1813–1826.
[6] B. Cao, Y. Wang, D. Wen, W. Liu, J. Wang, G. Fan, L. Ruan, B. Song, Y. Cai, M. Wei, X. Li, J. Xia, N. Chen, J. Xiang, T. Yu, T. Bai, X. Xie, L. Zhang, C. Li, Y. Yuan, H. Chen, H. Li, H. Huang, S. Tu, F. Gong, Y. Liu, Y. Wei, C. Dong, F. Zhou, X. Gu, J. Xu, Z. Liu, Y. Zhang, H. Li, L. Shang, K. Wang, K. Li, X. Zhou, X. Dong, Z. Qu, S. Lu, X. Hu, S. Ruan, S. Luo, J. Wu, L. Peng, F. Cheng, L. Pan, J. Zou, C. Jia, J. Wang, X. Liu, S. Wang, X. Wu, Q. Ge, J. He, H. Zhan, F. Qiu, L. Guo, C. Huang, T. Jaki, F.G. Hayden, P.W. Horby, D. Zhang, C. Wang, A trail of lopinavir-ritonavir in adults hospitalized with severe covid-19, N. Engl. J. Med. 382 (19) (2020) 1787–1799.
[7] J. Grein, N. Ohmagari, D. Shin, G. Diaz, E. Asperges, A. Castagna, T. Feldt, G. Green, M.L. Green, F.X. Lescure, E. Nicastri, R. Oda, K. Yo, E. Quiros-Roldan, A. Studemeister, J. Redinski, S. Ahmed, J. Bernett, D. Chelliah, D. Chen, S. Chihara, S.H. Cohen, J. Cunningham, A. D'Arminio Monforte, S. Ismail, H. Kato, G. Lapadula, E. L'Her, T. Maeno, S. Majumder, M. Massari, M. Mora-Rillo, Y. Mutoh, D. Nguyen, E. Verweij, A. Zoufaly, A.O. Osinusi, A. DeZure, Y. Zhao, L. Zhong, A. Chokkalingam, E. Elboudwarej, L. Telep, L. Timbs, I. Henne, S. Sellers, H. Cao, S.K. Tan, L. Winterbourne, P. Desai, R. Mera, A. Gaggar, R.P. Myers, D. M. Brainard, R. Childs, T. Flanigan, Compassionate use of remdesivir for patients with severe covid-19, N. Engl. J. Med. 382 (24) (2020) 2327–2336.
[8] J. Geleris, Y. Sun, J. Platt, J. Zucker, M. Baldwin, G. Hripcsak, A. Labella, D. Manson, C. Kubin, R.G. Barr, M.E. Sobieszczyk, N.W. Schluger, Observational study of hydroxychloroquine in hospitalized patients with covid-19, N. Engl. J. Med. 382 (25) (2020) 2411–2418.
[9] Y. Wang, D. Zhang, G. Du, R. Du, J. Zhao, Y. Jin, S. Fu, L. Gao, Z. Cheng, Q. Lu, Y. Hu, G. Luo, K. Wang, Y. Lu, H. Li, S. Wang, S. Ruan, C. Yang, C. Mei, Y. Wang, D. Ding, F. Wu, X. Tang, X. Ye, Y. Ye, B. Liu, J. Yang, W. Yin, A. Wang, G. Fan, Z. Fei, Z. Liu, X. Gu, J. Xu, L. Shang, Y. Zhang, L. Cao, T. Guo, Y. Wan, H. Qin, Y. Jiang, T. Jaki, F.G. Hayden, P.W. Hornby, B. Cao, C. Wang, Remdesivir in adults with severe COVID-19: a randomized, double-blind, placebo-controlled, multicenter trial, Lancet 395 (10236) (2020) 1569–1578.
[10] S.J. Park, K.M. Yu, Y.I. Kim, S.M. Kim, E.H. Kim, S.G. Kim, E.J. Kim, M.A.B. Casel, R. Rollon, S.G. Jang, M.H. Lee, J.H. Chang, M.S. Song, H.W. Jeong, Y. Choi, W. Chen, W.J. Shin, J.U. Jung, Y.K. Choi, Antiviral efficacies of FDA-approved drugs against SARS-CoV-2 infection in ferrets, mBio 11 (3) (2020) e01114–e01120.
[11] A. Zumla, J.F. Chan, E.L. Azhar, D.S. Hui, K.Y. Yuen, Coronaviruses - drug discovery and therapeutic options, Nat. Rev. Drug Discov. 15 (5) (2016) 327–347.
[12] H.A. Fozzard, M.F. Sheets, Cellular mechanism of action of cardiac glycosides, J. Am. Coll. Cardiol. 5 (Suppl A) (1985) 10A–15A.
[13] K.F. Benson, R.A. Newman, G.S. Jensen, Antioxidant, anti-inflammatory, anti-apoptotic, and skin regenerative properties of an Aloe vera-based extract of Nerium oleander leaves (NAE-8), Clin. Cosmet. Investig. Dermatol. 8 (2015) 239–248.
[14] Y. Pan, P. Rhea, L. Tan, C. Cartwright, H.J. Lee, M.K. Ravoori, C. Addington, M. Gagea, V. Kundra, S.J. Kim, R.A. Newman, P. Yang, PBI-05204, a supercritical CO_2 extract of Nerium oleander, inhibits growth of human pancreatic cancer via targeting the PI3K/mTOR pathway, Invest. New Drugs 33 (2015) 271–279.
[15] R.A. Newman, Y. Kondo, T. Yokoyama, S. Dixon, C. Cartwright, D. Chan, M. Johansen, P. Yang, Autophagic cell death of human pancreatic tumor cells mediated by oleandrin, a lipid-soluble cardiac glycoside, Integr. Cancer Ther. 6 (2007) 354–364.
[16] R.A. Newman, P. Yang, W.N. Hittelman, T. Lu, D.H. Ho, D. Ni, D. Chan, M. Vijjeswarapu, C. Cartwright, S. Dixon, E. Felix, C. Addington, Oleandrin-mediated oxidative stress in human melanoma cells, J. Exp. Ther. Oncol. 5 (2006) 167–181.

[17] D.S. Hong, H. Henary, G.S. Falchook, A. Naing, S. Fu, S. Moulder, J.J. Wheler, A. Tsimberidou, J.B. Durand, R. Khan, P. Yang, M. Johansen, R.A. Newman, R. Kurzrock, First-in-human study of PBI-05204, an oleander-derived inhibitor of AKT, FGF-2, NF-kappaBeta and p70s6k, in patients with advanced solid tumors, Invest. New Drugs 32 (2014) 1204–1212.
[18] M.T. Roth, D.B. Cardin, E.H. Borazanci, M. Steinbach, V.J. Picozzi, A. Rosemury, R. C. Wadlow, R.A. Newman, J. Berlin, A phase II, single-arm, open-label, bayesian adaptive efficacy and safety study of PBI-05204 in patients with stage IV metastatic pancreatic adenocarcinoma, Oncologist 25 (10) (2020) e1446–e1450.
[19] L. Amarelle, E. Lecuona, The antiviral effects of Na,K-ATPase inhibition: a minireview, IJMS 19 (8) (2018) 2154.
[20] R.A. Newman, K.J. Sastry, R. Arav-Boger, H. Cai, R. Matos, R. Harrod, Antiviral effects of oleandrin, J. Exp. Pharmacol. 12 (2020) 503–515.
[21] S. Singh, S. Shenoy, P.N. Nehete, P. Yang, B. Nehete, D. Fontenot, G. Yang, R. A. Newman, K.J. Sastry, Nerium oleander derived cardiac glycoside oleandrin is a novel inhibitor of HIV infectivity, Fitoterapia 84 (2013) 32–39.
[22] T. Hutchison, L. Yapindi, A. Malu, R.A. Newman, K.J. Sastry, R. Harrod, The botanical glycoside oleandrin inhibits human T-cell leukemia virus type-1 infectivity and env-dependent virological synapse formation, J. Antivir. Antiretrovir. 11 (3) (2019) 184.
[23] J.F. Chan, A.J. Zhang, S. Yuan, V.K. Poon, C.C. Chan, A.C. Lee, W.M. Chan, Z. Fan, H.W. Tsoi, L. Wen, R. Liang, J. Cao, Y. Chen, K. Tang, C. Luo, J.P. Cai, K.H. Kok, H. Chu, K.H. Chan, S. Sridhar, Z. Chen, H. Chen, K.K. To, K.Y. Yuen, Simulation of the clinical and pathological manifestations of coronavirus disease 2019 (COVID-19) in a golden syrian hamster model: implications for disease pathogenesis and transmissibility, Clin. Infect. Dis. 71 (9) (2020) 2428–2446.
[24] D.E. Dunn, D.N. He, P. Yang, M. Johansen, R.A. Newman, D.C. Lo, *In vitro* and *in vivo* neuroprotective activity of the cardiac glycoside oleandrin from Nerium oleander in brain slice-based stroke models, J. Neurochem. 119 (4) (2011) 805–814.
[25] T.P. Peacock, D.H. Goldhill, J. Zhou, L. Billon, R. Frise, O.C. Swann, R. Kugathasan, R. Penn, J.C. Brown, Y. Raul, S. David, L. Braga, M.K. Williamson, J.A. Hassard, E. Staller, B. Hanley, M. Osborn, M. Giacca, A.D. Davidson, D.A. Matthews, W.S. Barclay, The Furin Cleavage Site of SARS-CoV-2 Spike Protein is a Key Determinant for Transmission Due to Enhanced Replication in Airway Cells, 2020, bioRxiv, https://doi.org/10.1101/2020.09.30.318311.
[26] B.A. Johnson, X. Xie, B. Kalveram, K.G. Lokugamage, A. Muruato, J. Zou, X. Zhang, T. Juelich, J.K. Smith, L. Zhang, N. Bopp, C. Schindewolf, M. Vu, A. Vanderheiden, D. Swetnam, J.A. Plante, P. Aguilar, K.S. Plante, B. Lee, S.C. Weaver, M.S. Suthar, A.L. Routh, P. Ren, Z. Ku, Z. An, K. Debbink, P.Y. Shi, N.A. Freiberg, V.D. Menachery, Furin Cleavage Site Is Key to SARS-CoV-2 Pathogenesis, 2020, bioRxiv, https://doi.org/10.1101/2020.08.26.268854.
[27] J. Harcourt, A. Tamin, X. Lu, S. Kamili, S.K. Sakthivel, J. Murray, K. Queen, Y. Tao, C.R. Paden, J. Zhang, Y. Li, A. Uehara, H. Wang, C. Goldsmith, H.A. Bullock, L. Wang, B. Whitaker, B. Lynch, R. Gautam, C. Schindewolf, K.G. Lokugamage, D. Scharton, J.A. Plante, D. Mirchandani, S.G. Widen, K. Narayanan, S. Makino, T. G. Ksiazek, K.S. Plante, S.C. Weaver, S. Lindstrom, S. Tong, V.D. Menachery, N. J. Thornburg, Severe acute respiratory syndrome coronavirus 2 from patient with coronavirus disease, United States, Emerg. Infect. Dis. 26 (2020) 1266–1273.
[28] R.A. Newman, P. Yang, A.D. Pawlus, K.I. Block, Cardiac glycosides as novel cancer therapeutic agents, Mol. Interv. 8 (2008) 36–49.
[29] F. Perrotta, M.G. Matera, M. Cazzola, A. Bianco, Severe respiratory SARS-CoV2 infection: does ACE2 receptor matter? Respir. Med. 168 (2020), 105996.
[30] M.J. Van Kanegan, D.N. He, D.E. Dunn, P. Yang, R.A. Newman, A.E. West, D.C. Lo, BDNF mediates neuroprotection against oxygen-glucose deprivation by the cardiac glycoside oleandrin, J. Neurosci. 34 (2014) 963–968.
[31] L. Mao, H. Jin, M. Wang, Y. Hu, S. Chen, Q. He, J. Chang, C. Hong, Y. Zhou, D. Wang, X. Miao, Y. Li, B. Hu, Neurologic manifestations of hospitalized patients with coronavirus disease 2019 in Wuhan, China JAMA Neurol. 77 (6) (2020) 683–690.
[32] A.A. Asadi-Pooya, L. Simani, Central nervous system manifestations of COVID-19: a systematic review, J. Neurol. Sci. 413 (2020), 116832.
[33] P. Dey, T.K. Chaudhuri, Immunomodulatory activity of Nerium indicum through inhibition of nitric oxide and cyclooxygenase activity and modulation of TH1/TH2 cytokine balance in murine splenic lymphocytes, Cytotechnology 68 (2016) 749–761.
[34] C.T. Tseng, C. Huang, P. Newman, N. Wang, K. Narayanan, D.M. Watts, S. Makino, M.M. Packard, S.R. Zaki, T.S. Chan, C.J. Peters, Severe acute respiratory syndrome coronavirus infection of mice transgenic for the human Angiotensin-converting enzyme 2 virus receptor, J. Virol. 81 (2007) 1162–1173.
[35] M. Imai, K. Iwatsuki-Horimoto, M. Hatta, S. Loeber, P.J. Halfmann, N. Nakajima, T. Watanabe, M. Ujie, K. Takahashi, M. Ito, S. Yamada, S. Fan, S. Chiba, M. Kuroda, L. Guan, K. Takada, T. Armbrust, A. Balogh, Y. Furusawa, M. Okuda, H. Ueki, A. Yasuhara, Y. Sakai-Tagawa, T.J.S. Lopes, M. Kiso, S. Yamayoshi, N. Kinoshita, N. Ohmagari, S.I. Hattori, M. Takeda, H. Mitsuya, F. Krammer, T. Suzuki, Y. Kawaoka, Syrian hamsters as a small animal model for SARS-CoV-2 infection and countermeasure development, Proc. Natl. Acad. Sci. USA 117 (28) (2020) 16587–16595.
[36] Y.I. Kim, S.G. Kim, S.M. Kim, E.H. Kim, S.J. Park, K.M. Yu, J.H. Chang, E.J. Kim, S. Lee, M.A.B. Casel, J. Um, M.S. Song, H.W. Jeong, V.D. Lai, Y. Kim, B.S. Chin, J. S. Park, K.H. Chung, S.S. Foo, H. Poo, I.P. Mo, O.J. Lee, R.J. Webby, J.U. Jung, Y. K. Choi, Infection and rapid transmission of SARS-CoV-2 in ferrets, Cell Host Microbe 27 (2020) 704–709.e2.
[37] B. Rockx, T. Kuiken, S. Herfst, T. Bestebroer, M.M. Lamers, B.B. Oude Munnink, D. de Meulder, G. van Amerongen, J. van den Brand, N.M.A. Okba, D. Schipper, P. van Run, L. Leijten, R. Sikkema, E. Verschoor, B. Verstrepen, W. Bogers, J. Langermans, C. Drosten, M. Fentener van Vlissingen, R. Fouchier, R. de Swart, M. Koopmans, B.L. Haagmans, Comparative pathogenesis of COVID-19, MERS, and SARS in a nonhuman primate model, Science 368 (6494) (2020) 1012–1015.